NANO LETTERS

Letter

pubs.acs.org/NanoLett

Vertical Graphene Growth on SiO Microparticles for Stable Lithium Ion Battery Anodes

Liurong Shi,[†] Chunlei Pang,[‡] Shulin Chen,[§,∥] Mingzhan Wang,[†] Kexin Wang,[†] Zhenjun Tan,[†] Peng Gao,[§] Jianguo Ren,[‡] Youyuan Huang,[‡,⊥] Hailin Peng,*[,†] and Zhongfan Liu*[,†]

[†]Center for Nanochemistry (CNC), Beijing National Laboratory for Molecular Sciences, State Key Laboratory for Structural Chemistry of Unstable and Stable Species, College of Chemistry and Molecular Engineering, Peking University, Beijing 100871, P. R. China

[‡]BTR New Energy Materials Inc., Shenzhen 518106, P. R. China

[§]Electron Microscopy Laboratory, School of Physics, Peking University, Beijing 100871, P. R. China

[∥]State Key Laboratory of Advanced Welding and Joining, Harbin Institute of Technology, Harbin 150001, P. R. China

[⊥]Harbin Wanxin Graphite Valley Technology Co. Ltd., Harbin 150028, P. R. China

Supporting Information

ABSTRACT: Silicon-based materials are considered as strong candidates to next-generation lithium ion battery anodes because of their ultrahigh specific capacities. However, the pulverization and delamination of electrochemical active materials originated from the huge volume expansion (>300%) of silicon during the lithiation process results in rapid capacity fade, especially in high mass loading electrodes. Here we demonstrate that direct chemical vapor deposition (CVD) growth of vertical graphene nanosheets on commercial SiO microparticles can provide a stable conducting network via interconnected vertical graphene encapsulation during lithiation, thus remarkably improving the cycling stability in high mass loading SiO anodes. The vertical graphene encapsulated SiO (d-SiO@vG) anode exhibits a high capacity of 1600 mA h/g and a retention up to 93% after 100 cycles at a high areal mass loading of 1.5 mg/cm^2. Furthermore, 5 wt % d-SiO@vG as additives increased the energy density of traditional graphite/NCA 18650 cell by ∼15%. We believe that the results strongly imply the important role of CVD-grown vertical graphene encapsulation in promoting the commercial application of silicon-based anodes.

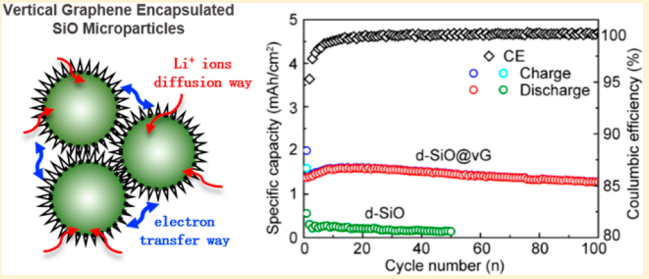

KEYWORDS: *Lithium ion battery, anode, SiO, vertical graphene, chemical vapor deposition*

To meet the ever-growing energy demands for advanced communication equipment and electric vehicles, intense efforts are continuously dedicated to lithium ion batteries with high energy density in the past decades.[1−4] Silicon-based materials (e.g., Si, SiO) are considered to be strong candidates of anode because of their ultrahigh specific capacity, natural abundance, and relatively low Li-uptake voltage.[5−9] However, the large volume expansions and contractions over repeated lithiation/delithiation processes always result in the pulverization and delamination of the active materials, which induces severe capacity decay due to the electrical isolations.[1] Among the diverse targeted strategies, silicon−carbon composites have been one of the most effective solutions to this problem.[10−15] In proper implementation, carbon material can impart its attractive properties to silicon-based materials. For instance, carbon materials are endowed with prominent mechanical flexibility and electrical conductivity; thus, they are capable of affording good tolerance to the volume expansion and preserving the electrical contacts during repeated lithiation/delithiation cycles.

Notably, the practical effects strongly depend on the carbon types and microscopic combination structures of silicon−carbon composites. Crystalline carbon materials (for instance, graphite, carbon nanotube, and graphene, etc.) are typically more effective than amorphous counterparts because of their higher electrical conductivity.[10,11,16−18] Specifically, graphene, with sp^2 bonded carbon atoms arranged in hexagonal 2D lattice, has significantly improved the performance of Si-based materials because of its superior electronic conductivity and mechanical flexibility.[19−22] However, because of its 2D planar structure with excellent impermeability, it could impede the lithium ion penetration when mixed improperly or used in excessive amounts.[16,23] Therefore, an effective graphene/silicon composite configuration is of paramount importance to fulfill the functions of graphene: (i) ensuring the electrical contact with surrounding conducting material as well as allowing fluent

Received: March 2, 2017
Revised: May 3, 2017
Published: May 4, 2017

DOI: 10.1021/acs.nanolett.7b00906
Nano Lett. 2017, 17, 3681−3687

Scheme 1. Design of Vertical Graphene Encapsulated Silicon-Based Microparticles[a]

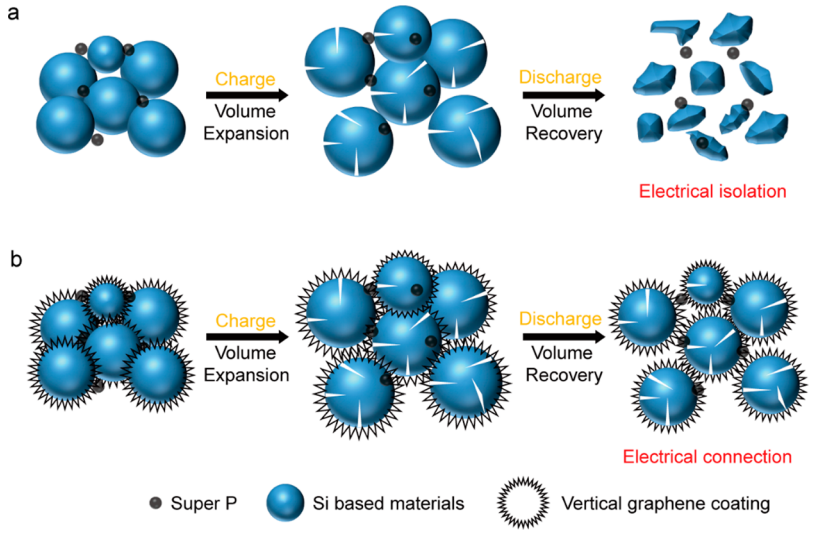

[a](a) Formation of electrical isolation in the silicon-based electrode during repeat battery cycling because of the volume expansion and recovery. (b) Vertical graphene encapsulation can provide a stable electrical connection between SiO particles during battery cycles via the interconnected vertical graphene nanosheets.

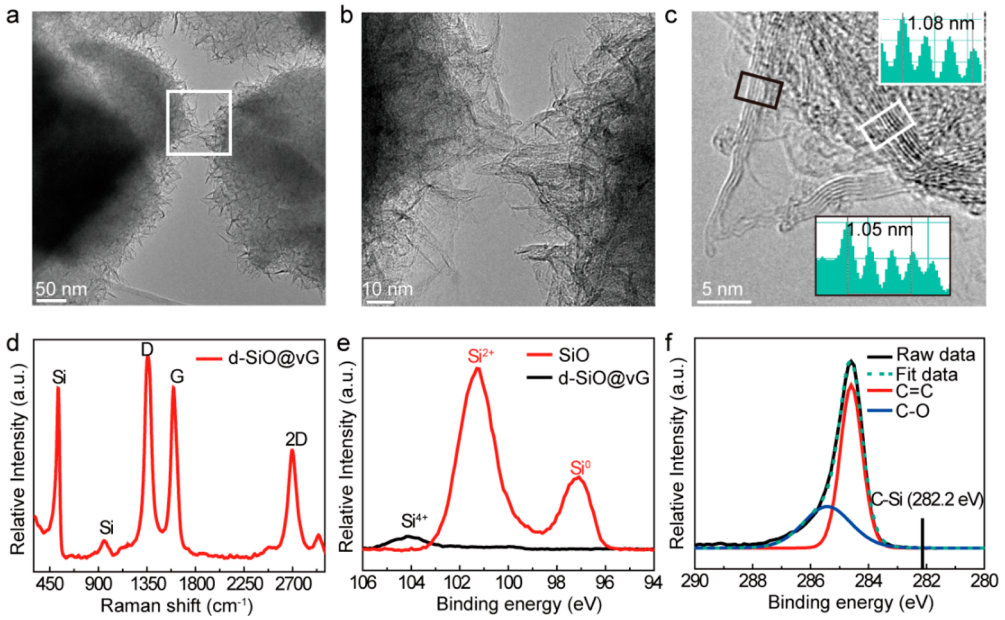

Figure 1. Vertical graphene growth on SiO microparticles. (a) TEM image of connected particles of d-SiO@vG. (b) Magnified image of the selected area in white box of panel a. (c) High-resolution TEM images of a vertical graphene sheet with a triangle shape. Insets are the line profiles from the marked boxes, respectively. (d) Raman spectra of d-SiO@vG. (e) XPS spectrum of the Si 2p band for d-SiO@vG and pristine SiO. (f) C 1s XPS spectrum of as-grown d-SiO@vG.

passage of lithium ions to active materials, (ii) buffering the volume change of silicon-based materials.

Herein, we report the vertical graphene encapsulation of silicon-based microparticles for stable lithium ion battery anode with a high specific capacity. The growth of vertical graphene on silicon monoxide (SiO) microparticles were realized by a facile and scalable chemical vapor deposition (CVD) process. The amorphous SiO_2 surface layer formed via the disproportion of SiO during the ramp-up period of heating not only provides numerous catalytic nucleation sites for the synthesis of graphene but also prevents the formation of SiC. The unique vertical graphene coating not only improves the electrical conductivity of SiO remarkably on the single particle level as well as on the electrode level but also provides ample transport channels of lithium ions. Consequently, the resultant silicon-based materials showed impressive stability (100 cycles, 93% retention) even at a high areal mass loading of 1.5 mg/cm^2. Besides, when used as additives, the capacity of commercial graphite/NCA 18650 cell was boosted from 2800 mA h to 3200 mA h by introducing only 5 wt % addition, manifesting great potential for industrial application.

The primary reason for the fast fading of capacity in silicon-based anodes is the loss of electrical contact in the electrode arising from the pulverization of particles and the isolation

DOI: 10.1021/acs.nanolett.7b00906
Nano Lett. 2017, 17, 3681−3687

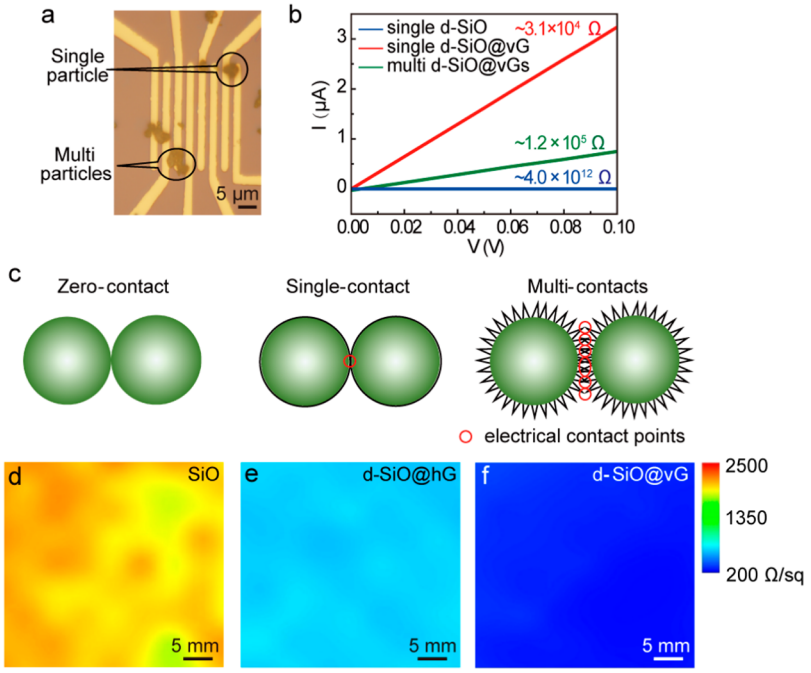

Figure 2. Conductivity measurements of d-SiO@vG particles. (a) Optical image of electrical circuit for current−voltage measurements of the particles. (b) $I-V_{ds}$ curves of single SiO, d-SiO@vG particles, and multiconnected d-SiO@vG particles. (c) Schematic illustration of electrical contacting mode between active materials. (d, e, f) 2D mapping images of the sheet resistance of the SiO (d), d-SiO@hG (e), and d-SiO@vG (f) composited electrode on PI film.

between particles during repeated cycles because of huge volume changes (Scheme 1a).[1] Herein, we introduce the vertical graphene encapsulation on silicon monoxide microparticles as ideal stabilizer. The vertical graphene encapsulation not only enhances the conductivity of single silicon monoxide particle but also provides the preserved connections between isolated particles after repeated cycles, which therefore guarantee the electrical connectivity (Scheme 1b). Hence, the capacity fade will be dramatically inhibited by introducing the vertical graphene encapsulation.

The direct growth of vertical graphene on commercial SiO microparticles was achieved by using methane as the carbon source in a facile CVD process. During the graphene synthesis, the SiO microparticles were simultaneously transformed into silicon and silica via a disproportionation reaction[24,25] (Figure S1). In the disproportionated SiO, silicon nanoparticles are embedded in the SiOx matrix, which can buffer the volume expansion, thus helpful for the cycling stability of SiO electrode (Figure S2). Figure 1a shows connected grown vertical graphene encapsulated disproportionated SiO microparticles (d-SiO@vG) (Figure S2). The close-up view clearly shows connections constructed by the vertical graphene nanosheets, which can work as the electron transfer pathways during the electrochemical process (Figure 1b). The height of vertical graphene nanosheets scales up with the increase of growth time (Figure S3). From the high-resolution transmission electron microscopy (HRTEM) observation, the graphene nanosheets exhibit triangle shapes, which is similar to the vertical graphene growth mode in plasmon enhanced CVD process. It is generally recognized that the vertical graphene growth starts from the formation of an amorphous carbon buffer layer. In this case, the big mismatch between the surface SiO_2 and graphene induced the formation of an amorphous carbon layer, which provide the nucleation sites for vertical graphene growth. The thermal cracking of methane supplies the carbon atoms needed for the graphene to grow upward.[26,27] (Figure 1c). The Raman spectrum shows the characteristic signals of graphene (D peak: ~1359 cm^{-1}, G peak: ~2699 cm^{-1}, and 2D peak: ~2690 cm^{-1}) (Figure 1d). The intense D-band is related to disorder and defects, which can be attributed to the numerous edges of the vertical graphene nanosheets.[28,29] The peaks located at 520 and 950 cm^{-1} originate from silicon nanocrystals formed via the disproportionation of SiO.[21,30] As evidenced by the screened intensity and upshift of silicon peak in the XPS spectrum (Figure 1e), the surface of the transformed substrate is mainly composed of amorphous SiO_2. The presence of C−O bond and absence of Si−C bond indicates the nucleation role of oxygen (Figure 1f) in the graphene growth.[31,32] We conclude that the transformation of the SiO substrate plays an important role on the growth of graphene. The SiO_2 skin layer not only provides numerous O sites for graphene nucleation but also acts as a barrier layer to prevent the formation of nonelectrochemical active SiC, which was proven critically challenging for the direct growth of carbon materials on silicon-based materials under high temperature.[20,30]

The conductivity of the electrochemical active materials plays an important role in its electrochemical performance. To substantiate the conducting characteristics of the vertical graphene coating layer, we examined its electrical behaviors on both the single-particle level and electrode level analyses (Figure 2a). Remarkably, the resistance of single silicon monoxide was strikingly decreased from ~4.0 × 10^{12} Ω to ~3.1 × 10^4 Ω with ca. 2.5 wt % graphene encapsulation (Figure 2b). Furthermore, the interconnections between multiparticles were proved highly conductive (Figure 2b, S4).

Considering the practical electrode manufacturing process, the resistivity of the composite was in close relation with the conductivity of single particle and the contact resistance between particles. According to conduction theory, the contact resistance will be decreased with the increase of electrical

DOI: 10.1021/acs.nanolett.7b00906
Nano Lett. 2017, 17, 3681−3687

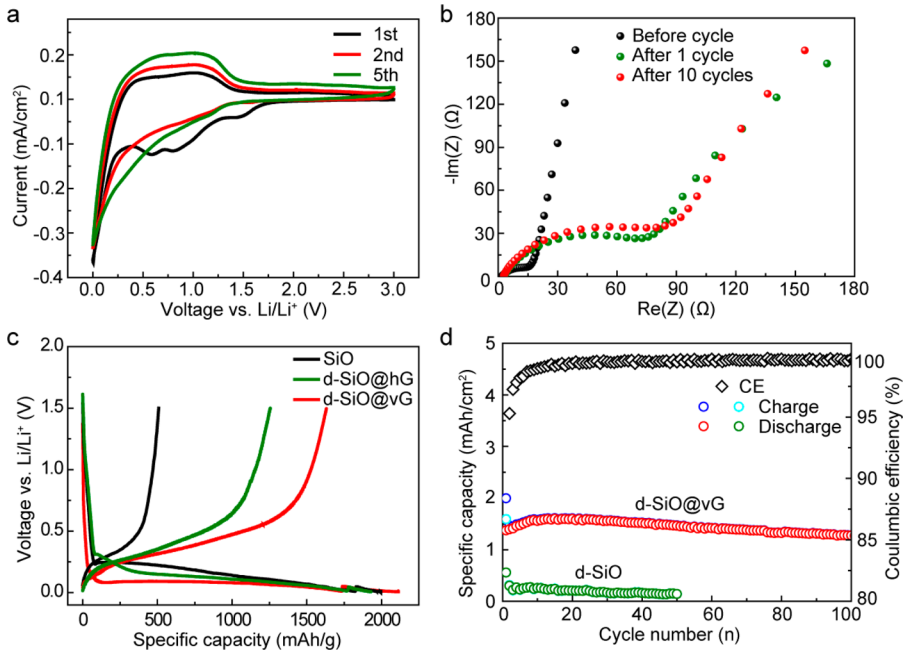

Figure 3. Electrochemistry performance of the d-SiO@vG anode. (a) Representative CV curves of d-SiO@vG electrode of the first, second, and fifth cycles. Scan rate: 0.05 mV s^{-1}. (b) Nyquist plots of d-SiO@vG electrodes before and after cycles. (c) Charge−discharge profiles at a current density of 160 mA/g. (d) Specific capacity and cycling efficiency of d-SiO and d-SiO@vG electrodes. The current density is 320 mA/g.

contact points.[26,33] A vertical graphene coating layer with a large surface area can provide more exposed graphene edges as contact points than that of pristine SiO and horizontal graphene layer coated disproportionated SiO particles (d-SiO@hG, Figure S5), and thus the contact resistance is largely decreased (Figure 2c). To evaluate the macroscopic conductivity of the electrode, the sheet resistances of the composited electrodes on insulating PI film were measured. As shown in Figure 2f, the d-SiO@vG electrode shows a uniform sheet resistance of ∼200 Ω/sq, much lower than that of d-SiO (∼2200 Ω/sq, Figure 2d) and d-SiO@hG based electrodes (∼700 Ω/sq, Figure 2e). As a consequence, the vertical graphene coating layer significantly facilitates the electron transport in the prepared anode enabled by the inherent fast electron transfer ability of pristine graphene coupled with effective contacts constructed by the interconnected vertical graphene sheets.

Due to the unique morphology of vertical graphene encapsulation, d-SiO@vG anode shows high capacity and cycling stability. The electrochemical performance of d-SiO@vG was examined in half-cell configuration where Li metal serves as the counter electrode. Figure 3a shows the first, second, and fifth cycles of the cyclic voltammetry (CV) profiles. The peak at 0.65 V in the cathodic scan of the first cycle that disappeared in the following cycles indicates a nonreversible reaction, namely, the formation of a stable solid electrolyte interphase (SEI) layer (Figure S6). The stability of SEI film was also evidenced by the Nyquist plot obtained from electrochemical impedance spectroscopy (EIS) tests, where the semicircle represents the charge transfer resistance. As shown in Figure 3b, the charge transfer resistance increased after the first cycle because of the formation of SEI film, while it remains nearly unchanged after 10 cycles. Besides the stable SEI film, the numerous freestanding vertical graphene nanosheets provide an increased specific surface area than that of pristine SiO (from 3 m^2/g to 12 m^2/g). The large electrode−electrolyte contact area facilitates the effective diffusion of both lithium ions and electrons to the d-SiO@vG particles, which results in an improved charge/discharge capacity[34] (Figure S7). As shown in Figure 3c, with the same carbon contents (2.5%), d-SiO@vG exhibits higher charge/discharge capacity than that of d-SiO@hG. The vertical graphene encapsulation makes a drastic improvement in the cycling performance (Figure 3d, S8). At a same areal mass loading of 1.5 mg/cm^2, the capacity retention of d-SiO was greatly improved from 28% to 93% after 50 cycles by simply vertical graphene encapsulating, indicating the prominent stabilizing function of vertical graphene encapsulation. After 100 cycles, the areal capacity of d-SiO@vG drops from 1.4 mA h/cm^2 to 1.3 mA h/cm^2. With such high areal capacity loading, the cycle stability (∼0.07% decay per cycle) is among the best cycling performances of silicon anodes reported to date. Although some publications have reported better stability than this work, the specific areal capacities (<1 mA h/cm^2) are quite low, which is far from the practical application requirements (Table S1). In the case of ultrahigh mass loading, the advantage of vertical graphene encapsulation is more significant. With same carbon contents of ca. 2.5 wt %, thus-obtained d-SiO@vG material shows higher cycling stability than that of d-SiO@hG even in the early cycles at a mass loading of 3.6 mg/cm^2, corresponding to an ultrahigh areal capacity of 5.8 mA h/cm^2, the highest areal capacity achieved to the best of our knowledge (Figure S6). These results strongly evidence the advantage of vertical graphene encapsulation, i.e., constructing stable conductive network via the interconnected vertical graphene nanosheets, thus prevent the capacity fading (Figure S9).

To reveal the structure evolution of d-SiO@vG particle during the lithiation process, a nanoelectrochemical cell was built in the TEM chamber, as illustrated in Figure 4a. The d-SiO@vG particles were placed onto a copper electrode and a movable tungsten electrode with LiO_2/Li at its tip was positioned in the opposite (Figure 4b). When they contact,

DOI: 10.1021/acs.nanolett.7b00906
Nano Lett. 2017, 17, 3681−3687

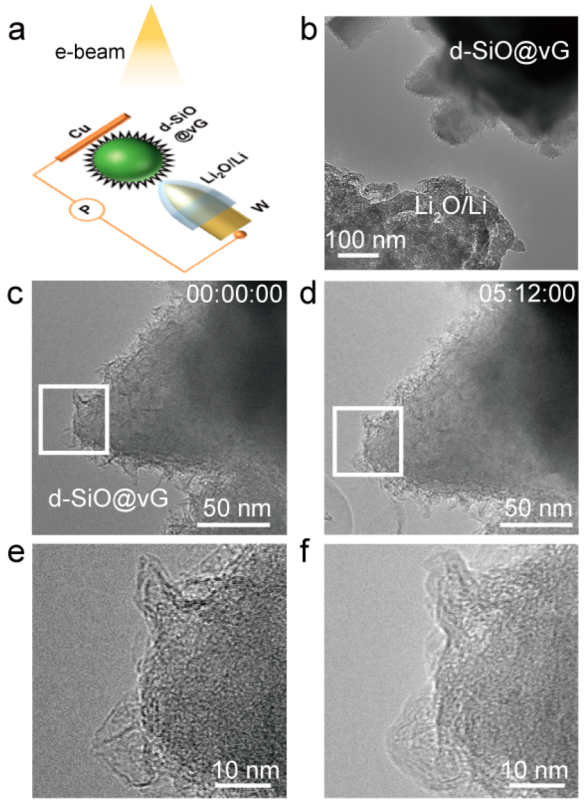

Figure 4. In situ TEM observation of d-SiO@vG particles during lithiation. (a, b) Schematic and TEM image of the nanoscale electrochemical cell for in situ lithiation. (c, d) The d-SiO@vG particle before (c) and after (d) lithiation. (e, f) The morphology of surface graphene coating layer of the marked areas in c and d, respectively.

the d-SiO@vG particle began to swell, indicating the insertion of lithium ions (Movie S1). At the end of lithiation, the length of d-SiO@vG particle increased by ~15% (~50% volume expansion, Figure 4c and d), much smaller than that of silicon monoxide particles, which was reported to be ~200%. The reduced volume expansion ratio can be ascribed to the synergistic clamping effects of the graphene and SiO_2 matrix. Moreover, from the in situ HRTEM observation, the vertical morphology of graphene coating layer remains almost the same before and after the expansion, indicating the preserved electrical pathways between the expanded particles (Figure 4e and f). This reflects the mechanical flexibility of the vertical graphene encapsulation, which is beneficial to the cycling stability of the d-SiO@vG anode.

It should be noted that previous publications only report the results tested by the half-cells, in which the specific capacity were normalized by the weight of the active materials. However, a high performance with practical value should be evaluated based on the total cell weight or volume. To further assess the practical viability of d-SiO@vG anode materials, it was mixed with commercial available graphite in a ratio of 5:95 as an anode to test its full cell performance. Standard 18650 type cylindrical batteries comprising a NCA ($LiNi_{0.8}Co_{0.15}Al_{0.05}O_2$) cathode and the d-SiO@vG/graphite anode were assembled (Figure 5a). At a discharge rate of 0.2 C, the cell shows a high capacity of 3200 mA h, 15% increased to graphite/NCA full cell, which is 2800 mA h (Figure S10). Because d-SiO@vG is only 5 wt % in the mixture with graphite, the energy density with respect to d-SiO@vG is 1200 Wh/kg, which is six times of 200 Wh/kg obtained for graphite/NCA 18650 full cell. Furthermore, the rate performance was measured by changing the discharge rates from 0.5 to 5 C as shown in Figure 5b, owing to the high conductivity and lithium ion permeability of the vertical graphene encapsulation, the capacity retention is up to 94% even at a high current density of 5 C. The cycling stability at a charge/discharging rate of 0.5 C/1 C (~80% after 400 cycles) meets the commercial cell standard (Figure 5c). However, we note that the percentage of d-SiO@vG cannot be improved because of intrinsic drawbacks of SiO particles like low initial Coulombic efficiency, which

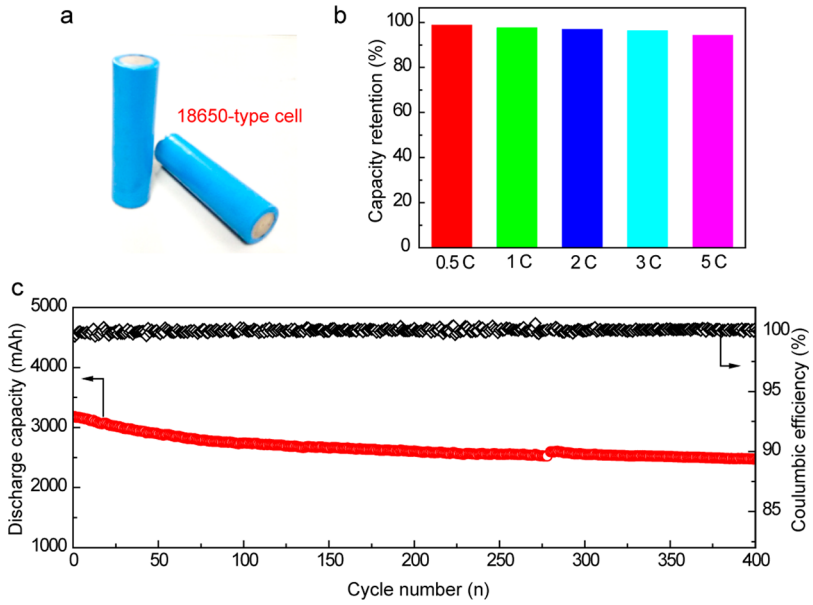

Figure 5. Performance of d-SiO@vG/graphite-NCA full cell. (a) Optical picture of the assembled 18650 full cells with the d-SiO@vG/graphite anode and the NCA cathode. (b) The rate performance of the assembled full cell under increasing charging C-rates from 0.5 to 5 C. (c) Cycling performance of the assembled full cell under charge/discharge rate of 0.5 C/1 C.

DOI: 10.1021/acs.nanolett.7b00906
Nano Lett. 2017, 17, 3681−3687

limits the further improvement of energy density. Relative efforts like prelithiation should be done to address this bottleneck problem.[35−37]

In conclusion, we realized the vertical graphene encapsulation on commercial SiO microparticles using a facile CVD method. The amorphous SiO_2 shin layer on the d-SiO particle formed during the disproportionation process plays an important role on the SiC-free growth of vertical graphene. More advanced than conventional horizontal carbon coating designs, the vertical graphene encapsulation fulfills the most rigorous demanded for surface coating of silicon based materials, that is, (i) constructing stable electrical contacts between active materials as well as the surrounding conducting material; (ii) enabling fluent passage of lithium ions to active materials; (iii) elastically buffering the volume change of silicon-based materials, thus resulting in a stable silicon-based anode especially in the case of high areal mass loading. Due to the high capacity and stability of d-SiO@vG, a 15% improvement in the energy density of graphite/NCA 18650 cell were achieved by introducing 5 wt % d-SiO@vG as additives. All in all, the current work not only provides a novel solution to address the capacity fade in lithium ion batteries from the point of material configuration engineering but also makes an important step toward the commercialization of silicon-based anodes.

Experimental Section. *CVD Process for Graphene Growth on SiO Microparticles.* The powder of SiO microparticles with an average diameter of 5 μm was provided by BTR new energy materials inc. The SiO powder was dispersed on a quartz plate and placed inside the furnace. The tube was purged with 300 sccm argon to remove air. Then the furnace was heated to 950 °C at a rate of 20 °C/min under Ar (300 sccm) and H_2 (30 sccm) flow at ambient pressure. The samples were then held at this temperature for 30, 60, 90, and 120 min under a constant mixed gas flow of argon (300 sccm), carbon source (4 sccm), and hydrogen (20 sccm) for graphene growth. After the furnace was cooled to room temperature, black powder was obtained. By using methane as carbon source, d-SiO@vG were obtained; by using ethanol as carbon source, d-SiO@hG were obtained. The carbon content were measured by carbon and sulfur analyzer. The prepared samples were characterized using optical microscopy (Olympus DX51 microscope), SEM (Hitachi S-4800; acceleration voltage 5−30 kV), TEM (FEI Tecnai F20; acceleration voltage 200 kV), Raman spectroscopy (Jobin Yvon LabRAM HR 800UV; 514.5 nm, 25 mW), XPS (Kratos, Axis Ultra, Mg Kα as the excitation source), and XRD (Phillips X' XPert Pro MPD; Cu Kα1 λ = 1.540598 Å, 40 kV, 100 mA).

In Situ TEM Experiment. For the in situ TEM experiments, all of the components were loaded onto a TEM specimen holder (PicoFemto) integrated with electrical biasing probe in argon-filled glovebox and then transferred into the TEM column using argon-filled plastic bag. During transferring the holder into the TEM chamber, the lithium metal was intentionally exposed to air for a few seconds to form a thin passivation layer of lithium oxide on the surface that acted as solid-state electrolyte to allow transport of lithium ions. The lithium insertion was initiated by applying a small negative bias between the tungsten probe and the grounded Cu grid. The dynamic process of lithiation was recorded by Oneview IS camera (Gatan) to form a movie.

Battery Preparation and Analysis. 2032-type stainless steel coin cells were used to assemble the test cells. For the preparation of the battery electrode, slurry was prepared by mixing pristine active material (d-SiO@vG, d-SiO@hG, d-SiO), Super P, and PVDF and in a weight ratio of 75:15:10 in NMP. The half-cell was then assembled by using lithium foil as both reference and counter electrodes. Clegard 2325 membrane and 1 M $LiPF_6$ in ethylene carbonate−dimethyl carbonate (1:1, v/v) were used as separator and electrolyte, respectively. The coin-type cell was assembled in an Ar-filled glovebox (MBraun Unilab). The electrochemical properties of cyclic voltammetry and electrochemical impedance spectroscopy were carried out on electrochemical workstation (Bio-Logic). The discharge and charge measurements of the batteries were performed on a Land (CT2001A) system under the voltage window between 0.01 and 1.5 V at room temperature. In the full cell fabrication, the N/P ratio is 1.04−1.05. The electrolyte is 1.2 M $LiPF_6$ in ethylene carbonate−ethyl methyl carbonate−dimethyl carbonate (1:1:3, v/v/v). The full cell performance of d-SiO@vG/graphite were characterized by paring with a NCA cathode.

Conductivity Measurements. A circuit was built by sandwiching the SiO and d-SiO@vG particles between two conducting Au electrodes to evaluate the conductivity of a single particle. By measuring the current as a function of applied voltage, we determined the corresponding electrical resistance of the individual particle. Slurry prepared by mixing pristine active material (d-SiO@vG, d-SiO@hG, SiO), Super P, and PVDF and in a weight ratio of 75:15:10 in NMP were lade coated on an insulating PI film. After a drying process, the sheet resistance of prepared electrode were measured by CDE ResMap model 178.

■ ASSOCIATED CONTENT

Supporting Information

The Supporting Information is available free of charge on the ACS Publications website at DOI: 10.1021/acs.nanolett.7b00906.

Further characterizations of d-SiO@vG and d-SiO@hG, and additional electrochemical results (Figure S1−10) (PDF)

Lithiation process of d-SiO@vG (Movie S1) (AVI)

■ AUTHOR INFORMATION

Corresponding Authors

*E-mail: zfliu@pku.edu.cn.

*E-mail: hlpeng@pku.edu.cn.

ORCID

Peng Gao: 0000-0003-0860-5525

Hailin Peng: 0000-0003-1569-0238

Zhongfan Liu: 0000-0003-0065-7988

Notes

The authors declare no competing financial interest.

■ ACKNOWLEDGMENTS

This work was financially supported by Beijing Municipal Science & Technology Commission (nos. Z161100002116002), the National Basic Research Program of China (nos. 2014CB932500 and 2016YFA0200101, 2013CB932603), the National Natural Science Foundation of China (nos. 21525310, 51432002, and 51520105003), and National Program for Support of Top-Notch Young Professionals.

DOI: 10.1021/acs.nanolett.7b00906
Nano Lett. 2017, 17, 3681−3687

REFERENCES

(1) Choi, J. W.; Aurbach, D. *Nat. Rev. Mater.* **2016**, *1* (4), 16013.
(2) Jiang, J.; Li, Y.; Liu, J.; Huang, X.; Yuan, C.; Lou, X. W. *Adv. Mater.* **2012**, *24* (38), 5166−5180.
(3) Larcher, D.; Tarascon, J. M. *Nat. Chem.* **2014**, *7* (1), 19−29.
(4) Sun, Y.; Liu, N.; Cui, Y. *Nature Energy* **2016**, *1* (7), 16071.
(5) Li, X.; Gu, M.; Hu, S.; Kennard, R.; Yan, P.; Chen, X.; Wang, C.; Sailor, M. J.; Zhang, J. G.; Liu, J. *Nat. Commun.* **2014**, *5*, 4105.
(6) Wang, C. M.; Li, X.; Wang, Z.; Xu, W.; Liu, J.; Gao, F.; Kovarik, L.; Zhang, J. G.; Howe, J.; Burton, D. J.; Liu, Z.; Xiao, X.; Thevuthasan, S.; Baer, D. R. *Nano Lett.* **2012**, *12* (3), 1624−1632.
(7) Szczech, J. R.; Jin, S. *Energy Environ. Sci.* **2011**, *4* (1), 56−72.
(8) Kasavajjula, U.; Wang, C.; Appleby, A. J. *J. Power Sources* **2007**, *163* (2), 1003−1039.
(9) McDowell, M. T.; Lee, S. W.; Nix, W. D.; Cui, Y. *Adv. Mater.* **2013**, *25* (36), 4966−4985.
(10) Liu, X.; Du, Y.; Hu, L.; Zhou, X.; Li, Y.; Dai, Z.; Bao, J. *J. Phys. Chem. C* **2015**, *119* (11), 5848−5854.
(11) Zhou, X.; Yin, Y.-X.; Wan, L.-J.; Guo, Y.-G. *Adv. Energy Mater.* **2012**, *2* (9), 1086−1090.
(12) Liu, N.; Lu, Z.; Zhao, J.; McDowell, M. T.; Lee, H. W.; Zhao, W.; Cui, Y. *Nat. Nanotechnol.* **2014**, *9* (3), 187−192.
(13) Li, M.; Yu, Y.; Li, J.; Chen, B.; Wu, X.; Tian, Y.; Chen, P. *J. Mater. Chem. A* **2015**, *3* (4), 1476−1482.
(14) Kim, J.-H.; Sohn, H.-J.; Kim, H.; Jeong, G.; Choi, W. *J. Power Sources* **2007**, *170* (2), 456−459.
(15) Wu, W.; Liang, Y.; Ma, H.; Peng, Y.; Yang, H. *Electrochim. Acta* **2016**, *187*, 473−479.
(16) Su, F.-Y.; He, Y.-B.; Li, B.; Chen, X.-C.; You, C.-H.; Wei, W.; Lv, W.; Yang, Q.-H.; Kang, F. *Nano Energy* **2012**, *1* (3), 429−439.
(17) Raccichini, R.; Varzi, A.; Passerini, S.; Scrosati, B. *Nat. Mater.* **2014**, *14* (3), 271−9.
(18) Chen, Z.; Ren, W.; Gao, L.; Liu, B.; Pei, S.; Cheng, H. M. *Nat. Mater.* **2011**, *10* (6), 424−8.
(19) Bonaccorso, F.; Colombo, L.; Yu, G.; Stoller, M.; Tozzini, V.; Ferrari, A. C.; Ruoff, R. S.; Pellegrini, V. *Science* **2015**, *347* (6217), 1246501.
(20) Son, I. H.; Hwan Park, J.; Kwon, S.; Park, S.; Rummeli, M. H.; Bachmatiuk, A.; Song, H. J.; Ku, J.; Choi, J. W.; Choi, J. M.; Doo, S. G.; Chang, H. *Nat. Commun.* **2015**, *6*, 7393.
(21) Li, Y.; Yan, K.; Lee, H.-W.; Lu, Z.; Liu, N.; Cui, Y. *Nature Energy* **2016**, *1* (2), 15029.
(22) David, L.; Bhandavat, R.; Barrera, U.; Singh, G. *Nat. Commun.* **2016**, *7*, 10998.
(23) Wei, W.; Lv, W.; Wu, M.-B.; Su, F.-Y.; He, Y.-B.; Li, B.; Kang, F.; Yang, Q.-H. *Carbon* **2013**, *57*, 530−533.
(24) Lee, J.-I.; Choi, N.-S.; Park, S. *Energy Environ. Sci.* **2012**, *5* (7), 7878.
(25) Hirata, A.; Kohara, S.; Asada, T.; Arao, M.; Yogi, C.; Imai, H.; Tan, Y.; Fujita, T.; Chen, M. *Nat. Commun.* **2016**, *7*, 11591.
(26) Bo, Z.; Zhu, W.; Ma, W.; Wen, Z.; Shuai, X.; Chen, J.; Yan, J.; Wang, Z.; Cen, K.; Feng, X. *Adv. Mater.* **2013**, *25* (40), 5799−806.
(27) Zhao, J.; Shaygan, M.; Eckert, J.; Meyyappan, M.; Rummeli, M. H. *Nano Lett.* **2014**, *14* (6), 3064−71.
(28) Ferrari, A. C.; Meyer, J. C.; Scardaci, V.; Casiraghi, C.; Lazzeri, M.; Mauri, F.; Piscanec, S.; Jiang, D.; Novoselov, K. S.; Roth, S.; Geim, A. K. *Phys. Rev. Lett.* **2006**, *97* (18), 187401.
(29) Bokobza, L.; Bruneel, J.-L.; Couzi, M. C. *J. Carbon Res.* **2015**, *1* (1), 77−94.
(30) Chen, J.; Wen, Y.; Guo, Y.; Wu, B.; Huang, L.; Xue, Y.; Geng, D.; Wang, D.; Yu, G.; Liu, Y. *J. Am. Chem. Soc.* **2011**, *133* (44), 17548−51.
(31) Chen, K.; Li, C.; Shi, L.; Gao, T.; Song, X.; Bachmatiuk, A.; Zou, Z.; Deng, B.; Ji, Q.; Ma, D.; Peng, H.; Du, Z.; Rummeli, M. H.; Zhang, Y.; Liu, Z. *Nat. Commun.* **2016**, *7*, 13440.
(32) Shi, L.; Chen, K.; Du, R.; Bachmatiuk, A.; Rummeli, M. H.; Xie, K.; Huang, Y.; Zhang, Y.; Liu, Z. *J. Am. Chem. Soc.* **2016**, *138* (20), 6360−6363.
(33) Li, L.; Morris, J. E. *IEEE Trans. Compon., Packag., Manuf. Technol., Part A* **1997**, *20*, 3.
(34) Zhang, Q.; Tan, S.; Mendes, R. G.; Sun, Z.; Chen, Y.; Kong, X.; Xue, Y.; Rummeli, M. H.; Wu, X.; Chen, S.; Fu, L. *Adv. Mater.* **2016**, *28* (13), 2616−2623.
(35) Liu, N.; Hu, L.; McDowell, M. T.; Jackson, A.; Cui, Y. *ACS Nano* **2011**, *5* (8), 6487−6493.
(36) Kim, H. J.; Choi, S.; Lee, S. J.; Seo, M. W.; Lee, J. G.; Deniz, E.; Lee, Y. J.; Kim, E. K.; Choi, J. W. *Nano Lett.* **2016**, *16* (1), 282−288.
(37) Forney, M. W.; Ganter, M. J.; Staub, J. W.; Ridgley, R. D.; Landi, B. J. *Nano Lett.* **2013**, *13* (9), 4158−4163.

DOI: 10.1021/acs.nanolett.7b00906
Nano Lett. 2017, 17, 3681−3687